ZnO-based ternary compound nanotubes and nanowires†

Hong Jin Fan,*[a] Yang Yang[b] and Margit Zacharias[c]

Received 23rd July 2008, Accepted 24th October 2008
First published as an Advance Article on the web 16th December 2008
DOI: 10.1039/b812619d

In the last few years nanostructure ZnO is being intensively investigated from the growth control, structural and physical characterization, to device performance. There are now increasing interests in a wide range of ZnO-based ternary compound nanostructures offering even larger possibilities. These compounds can be useful as multi-color light-emitting device, sensors, transparent electrodes, or catalysts. This Review summarizes typical ZnO-based ternary compound nanotubes and nanowires, which are fabricated based on either solid-state reactions with ZnO and/or porous templates, or on the vapour-liquid-solid process. Our focus is put on spinel-type compounds formed with oxides like Al_2O_3, Ga_2O_3, Fe_2O_3, Sb_2O_3, TiO_2, and SnO_2. The discussion includes the growth strategies, nanosize effects, and the associated reaction mechanisms. ZnMgO alloy nanowires, another technologically important ternary compound, are touched at the end, too.

Introduction

Among the one-dimensional (1-D) nanoscale semiconductors, ZnO is the most studied material compared to Si, Ge, and III–V materials, driven by the relatively simple and cheap growth setup, high growth throughput, and multi-functionality of nanostructured ZnO and its derivatives. Prospectively ZnO itself holds a wide range of applications because of its wide bandgap (3.37 eV) semiconductivity, large exciton binding energy (60 meV) and piezoelectricity ($d_{33} \approx 12$ pC/N). Research on nanostructured ZnO has boomed since 2001 when Wang[1] and Yang[2] reported respectively ZnO nanobelts and nanowires. Worldwide there are numerous groups devoted to basic research on ZnO in its various morphologies from thin films, quantum wells to nanostructures. The number of published works on ZnO-based nanostructure is increasing every day, ranging from growth, physical characterization, device testing, to theoretical simulations. Besides thousands of original papers, there are also a good number of review articles available. Listed below are some journal reviews:

- *Zinc oxide nanostructures: growth, properties and applications* – Wang (2004)[3]
- *ZnO nanowire growth and devices* – Heo (2004)[4]
- *A comprehensive review of ZnO materials and devices* – Özgür (2005)[5]
- *ZnO nanorods: synthesis, characterization and applications* – Yi (2005)[6]
- *Zinc Oxide Nanostructures: Synthesis and Properties* – Fan (2005)[7]

[a]*Division of Physics and Applied Physics, School of Physical & Mathematic Sciences, Nanyang Technological University, 21 Nanyang Link, 637371, Singapore. E-mail: fanhj@ntu.edu.sg*
[b]*Max Planck Institute of Microstructure Physics, 06120 Weinberg 2, Halle, Germany*
[c]*Faculty of Applied Science (IMTEK), Albert-Ludwigs-University Freiburg, Georges-Köhler-Allee, 79110 Freiburg, Germany*
† This paper is part of a *Journal of Materials Chemistry* theme issue on Nanotubes and Nanowires. Guest editor: Z. L. Wang.

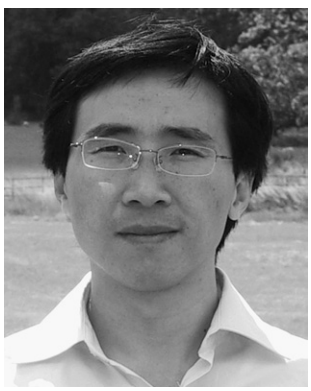

Hong Jin Fan

H. J. Fan received his Ph.D. from National University of Singapore in 2003. After that he was a postdoc at Max-Planck-Institute of Microstructure Physics, Germany, focusing on ZnO-based nanowire arrays and tubular nanostructures, and later at University of Cambridge working with Prof. J. F. Scott. Since 2008 he has been an assistant professor in Nanyang Technological University. His research interests include fabrication, optical and electronic properties of inorganic nanowires and nanotubes.

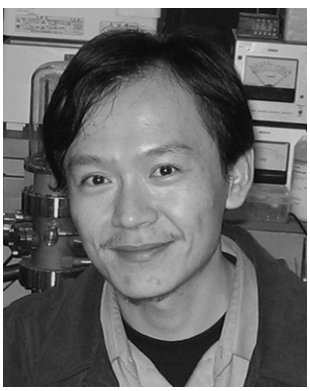

Yang Yang

Y. Yang received his B.S. (1997) and Ph.D. (2003) degrees in chemistry from Nanjing University, China. From 2004 to 2006, he was a JSPS fellow at University of Hyogo, Japan, focusing on self-assembly of metal and semiconductor nanoparticles. Since 2006, he has been a postdoc researcher at MPI of Microstructure Physics, Germany. His research interests include semiconductor nanowires and nanotubes, compound oxide nanostructures, atomic layer depositions and self-assembly of nanomaterials.

• *Semiconductor nanowires: from self-organization to patterned growth* – Fan (2006)[8]
• *Optical Properties of ZnO Nanostructures* – Djurišić (2006)[9]
• *Nanowire and nanobelt arrays of zinc oxide: from synthesis to properties and to novel devices* – Wang (2007)[10]
• *ZnO: From basics towards applications* – Klingshirn (2007)[11]
• *ZnO – nanostructures, defects, and devices* – Schmidt-Mende (2007)[12]

The main attention on 1-D ZnO nanostructures is focused on their structural, optical and optoelectronic properties. Also, due to the easy availability, ZnO nanowires have been widely used as physical (non-reactive) templates for the fabrication of nanotubes like single-crystalline GaN,[13] amorphous alumina[14] and silica,[15] and Pt–$BaTiO_3$–Pt double-electroded ferroelectrics.[16]

In most cases, compounds based on ZnO are technologically more important than its pure phase. For example, alloying with Cd or Mg is an effective route to tuning the optical bandgap of ZnO; doping with lithium or vanadium has been shown to enhance the piezoelectricity, because the spontaneous polarization (due to the non-centrosymmetric crystal structure $P6_3mc$) is enlarged by replacing Zn ions by smaller Li or V ions which causes lattice distortions;[17,18] alloying ZnO with In_2O_3 gives thermoelectric applications.[19] Most of the work is still on bulk materials or films for their potential applications like SAW (surface acoustic wave) devices, piezoelectric actuators, and transparent conductors.

ZnO can form spinel type ternary compounds with many other oxides. They have a formula of either $ZnM_2^{[3+]}O_4$or $Zn_2M^{[4+]}O_4$ (M = Al, Ga, Fe, In, Sn, Sb, Ti, Mn, V, Cr), and can be formed through either solid-state reactions by thermal annealing, or hydrothermal growth, or in-situ vapor-liquid-solid (VLS) growth by co-evaporating powders of the constituent oxides. There is now increasing interest in ZnO-based spinel 1-D nanostructures within the domain of ZnO research (see Table 1). Such nanoscale materials show a large diversity of morphologies, such as tubes, wires, periodically zigzagged and/or twinned wires, which might reflect the uniqueness of the nanoscale solid-state reaction (versus bulk reactions) and VLS growth of ternary compound nanowires (versus binary compounds). Some basic phenomena like growth dynamics and diffusion mechanism can be adapted from those well understood bulk materials, but obviously not all. Because of a large surface-to-volume ratio and symmetry breaking on the surface, nanoscale spinel oxides have shown physical properties different from the bulk counterparts. Most of them are wide bandgap semiconductors and typical phosphorous materials.

This feature article gives a material-by-material summary of the so-far demonstrated examples of ternary 1-D ZnO-based nanostructures, with a focus on spinels. We will discuss the merits and drawbacks of the fabrication routes, analyze the common feature of the structures particularly the twinned nanowires, and also point out the potential spinel-forming interface reaction problem which is up to now not so well known in the ZnO nanowire community and hence may not have been considered.

Margit Zacharias

Since 2007, M. Zacharias has been a Professor of Nanotechnology at the Faculty of Applied Science (IMTEK), Freiburg University, Germany. Before that she was a Professor at Paderborn University and a group leader at MPI of Microstructure Physics, Halle. Since June 2004, she has coordinated the Germany priority program on nanowires and nanotubes (SPP 1165). Her research interests include nanocrystalline silicon, ZnO nanowires, and their investigation, understanding, and applications.

Basics of spinels

AB_2O_4 type spinels have a cubic lattice structure, which at low temperatures consists of an fcc sublattice of O with divalent cations (A^{2+}) occupying one-eighth of the tetrahedral interstices and the trivalent cations (B^{3+}) occupying one half of the octahedral interstices (see Fig. 1). One conventional unit cell comprises 8 formula units: 8 A metal cations, 16 B metal cations and 32 O anions. The divalent, trivalent, or quadrivalent metal cations can be Mg, Zn, Fe, Mn, Al, Cr, Ti, and V. Some crystals have an inverse spinel structure, which contains only half of the B^{3+} cations at tetrahedral sites while the other half of the B^{3+} and all the A^{2+} are at octahedral sites, *i.e.* $B^{3+}(A^{2+}B^{3+})O_4$. A review article on spinel crystal structures was written by Sickafus, Wills and Grimes.[20]

Solid-state reactions of type $AO + B_2O_3 \rightarrow AB_2O_4$ are a common way for the fabrication of spinel oxides. Traditional studies on spinel-formation reactions are usually conducted at planar interfaces or in the form of powder mixtures by bringing two solid binary oxides, or a solid oxide and a vapor or liquid phase, into contact at high temperatures (>1000 °C).[21] The growth process of classical spinel oxides involves the so-called Wagner's cation counterdiffusion mechanism,[22,23] viz. cations migrating through the reaction interface in opposite directions and the oxygen sublattice remaining essentially fixed (see Fig. 2a). This mechanism applies to many types of spinels, for example, $ZnFe_2O_4$, $MgAl_2O_4$, Mg_2TiO_4. The reaction $MgO + Al_2O_3 \rightarrow MgAl_2O_4$ has long been a model system for the study of reaction thermodynamics and kinetics. Recently fabrication of single-crystalline $MgAl_2O_4$ nanowires[24] and nanotubes[25] has been reported. MgO is cubic with a lattice constant (0.42 nm) about half of most cubic spinels (*e.g.*, 0.81 nm for $MgAl_2O_4$): also it has the same fcc-type oxygen sublattice as that in cubic spinels. Therefore, spinels grown on the MgO substrate usually have good interface lattice coherence and are single crystalline. In other cases when the two oxides are non-cubic, the O sublattice has to rearrange from, e.g., hcp in sapphire, to fcc cubic, which easily results in grain growth of different orientations and a rough interface.

The reaction of ZnO (wurtzite structure, $a = 0.3250$ nm, $c = 0.5207$ nm) with Al_2O_3 into $ZnAl_2O_4$ spinel (cubic structure, $a = 0.880$ nm) is, however, unique: the growth mechanism involves

Table 1 A summary of spinel-type ternary oxide one-dimensional nanostructures based on ZnO

Material	Nanomorphology	Formation process	Ref.
$ZnAl_2O_4$	Linked tubes	Reaction of porous alumina with Zn vapor	33,34
	Tubes	Reaction of porous alumina with Zn precursor in liquids	35
	Tubes	Solid-state reaction of core-shell nanowires	36,39,40
$ZnGa_2O_4$	Wires	Thermal evaporation of powder mixture and vapor-liquid-solid	51,52
	Helical wires and springs	Thermal evaporation of powder mixture and vapor-liquid-solid	53
	Shells with Ga_2O_3 core	Solid-state reaction of Ga_2O_3 nanowires with Zn vapor	54
	Tubes	Solid-state reaction of ZnO nanowires with Ga–O vapor and removal of ZnO core	55
Zn_2TiO_4	Twinned wires	Solid-state reaction of ZnO/Ti core/shell nanowires	58
	Twinned wires	Solid-state reaction of ZnO/TiO_2 core/shell nanowires	[b]
Zn_2SnO_4	Belts or ribbons	Thermal evaporation of powder mixture and vapor-solid	65,67
	Rings	Thermal evaporation of powder mixture and vapor-solid	65
	Chainlike zigzag but single-crystalline	Thermal evaporation of ZnO/SnO powder	63,66,68
	Twinned zigzag wires	Thermal evaporation of ZnO/SnO powder	63,64,66,69
	Thin rods	Hydrothermal synthesis	70
$ZnSb_2O_4$	Wires and belts	Thermal evaporation of powder mixture and deposition	118
$ZnCr_2O_4$	Tubes of granular wall	Reaction of Zn nanowires with CrO_2Cl_2 vapor	94
$ZnFe_2O_4$	Chainlike wires	Infiltration of nanoparticles into porous alumina and ripening	88
	Wires	Solution infiltration in silica template	89
	Shells	Solid-state reaction of ZnO/Fe_2O_3 core/shell wires	[b]
Zn_2SiO_4[a]	Brushes	Reaction with surfactant-assembled mesoporous silica template	98
	Porous shell	Reaction of ZnO nanowires with Si vapor	99
	Tubes	Solid-state reaction of ZnO/Si core/shell nanowires	100
Zn_2GeO_4[a]	Rods	Nucleation from the amorphous membranes composed of Ge, Zn and O during aging	103

[a] They have an AB_2O_4 formula but are not spinel-type structure. [b] Unpublished data.

the diffusion of both Zn and O and an effective unilateral transfer of ZnO into the spinel (see Fig. 2b). This was first pointed out by Bengtson and Jagitsch,[26] and later readdressed by Navias,[27] Branson[28] and Keller *et al.*[29] This means that an inert marker plane placed at the initial interface will be found at the ZnO/spinel interface for the ZnO–Al_2O_3 reaction, whereas in case of the MgO–Al_2O_3 reaction, the marker plane is within the spinel layer.

In bulk solid-state reactions, the diffusion of atoms through the growing product phase generally represents the rate-controlling step; therefore a high annealing temperature and long time are usually needed for a complete sintering reaction. But a temperature higher than 1300 °C results in stoichiometric problems because of the volatility of the reactants, *e.g.*, ZnO. In a nanoscale system, the diffusion path is shortened so that the reaction steps at the interface may become rate controlling. Furthermore, during the growth of hollow nanoparticles or nanotubes, surface diffusion and grain boundary diffusion can become the dominating transport process over the volume diffusion. Adding up these aspects, the sintering temperature and time can be reduced for nanoscale solid-state reactions.

A mandatory condition to grow single-crystalline spinel films is that one of the oxides should be a single-crystal substrate. Likewise, for nanoscale spinel-forming solid-state reactions, a single-crystalline nanowire is commonly used as a "single-crystalline substrate". The examples listed in Table 1 mainly use

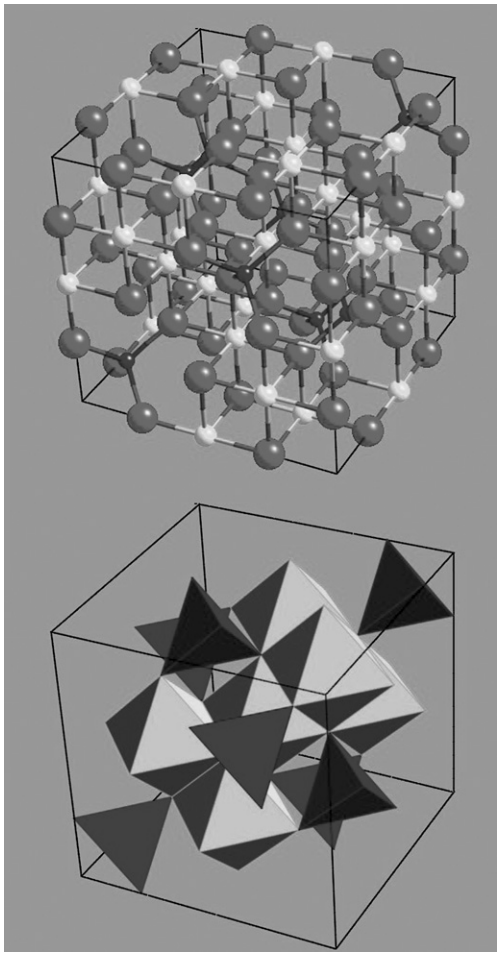

Fig. 1 (Top) Ball-and-stick and (bottom) polyhedral model of the AB_2O_4 spinel structure. Cations A are located at tetrahedral interstices and surrounded by 4 oxygens; whereas cations B are at octahedral interstices and surrounded by 6 oxygens. The oxygen atoms have an fcc-type close packed sublattice occupying the corners of the polyhedra.

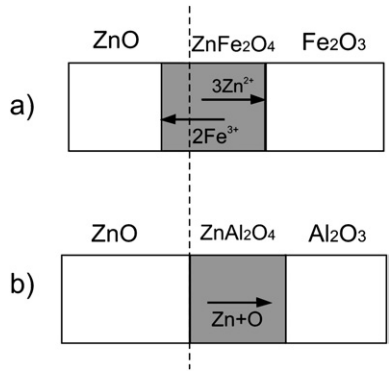

Fig. 2 Schematics of the two main diffusion mechanisms during the spinel-forming solid-state reactions. (a) Wagner counterdiffusion. Typical reaction is ZnO–Fe_2O_3 and MgO–Al_2O_3. (b) Uni-directional diffusion. Typical reaction is ZnO–Al_2O_3. The dashed line indicates the initial interface. An inert marker plane placed at the initial interface will be found at the ZnO/spinel interface in (b), and within the spinel layer in (a), dividing this layer in a ratio of 1:3 as a result of charge neutrality of the overall diffusion flux.

ZnO nanowires as the starting material which are always single-crystalline because of the either a vapour- or liquid-phase synthesis process.

$ZnAl_2O_4$

The initial idea of coating a ZnO nanowire with a thin layer of Al_xO_y was a surface passivation layer to reduce the unwanted surface charge recombination. Two independent studies[30,31] have shown that an Al_xO_y cap layer efficiently lowers the defect-related deep level emissions. Such alumina capping appears helpful for the application of ZnO nanowires as photo electrodes in dye-sensitized solar cells by reducing the recombination of photo-generated electron–hole pairs on the nanowire surface.[32]

Porous aluminium oxide is known as a typical morphology-defining template for fabrication of 1-D nanostructures. When in contact with ZnO, however, alumina is also one of the reactants to form $ZnAl_2O_4$ (ZAO, zinc aluminate) spinel. Wang *et al.*[33,34] and Zhao *et al.*[35] obtained ZAO nanotubes by reacting a Zn-containing precursor with the porous alumina template (see Fig. 3). In Wang's experiment, Zn vapor was generated by H_2 reduction of ZnO or ZnS powder; whereas no spinel was formed using the pristine ZnO solid source because of insufficient contact. Overall single-crystalline ZAO nanonets were obtained after annealing at 680 °C for 1000 min[33] or 650–660 °C for

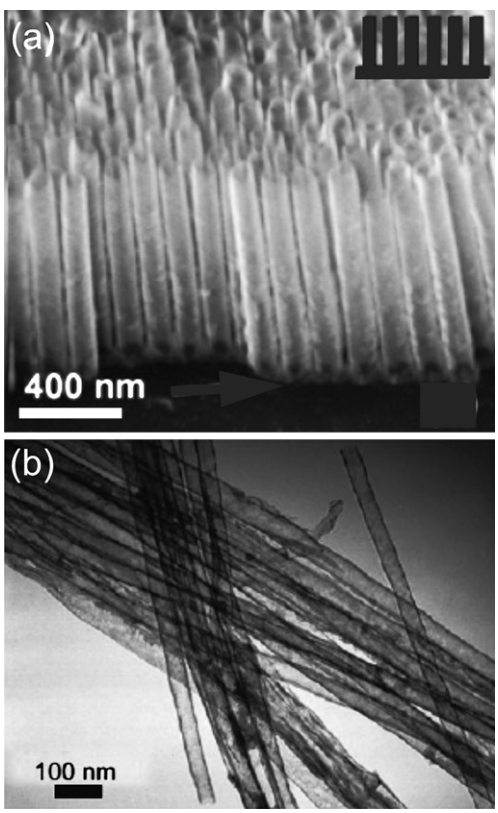

Fig. 3 $ZnAl_2O_4$ obtained by reacting Zn precursor with porous alumina templates. (a) Single-crystal nanonet. Reprinted with permission.[33] Copyright 2005 American Chemical Society. (b) Polycrystalline nanotubes. Copyright Wiley-VCH Verlag GmbH & Co. KGaA. Reprinted with permission.[35]

800 min.[34] Variation of the tube wall thickness was realized by varying the temperature and reaction time, but restrained below 20 nm because of the limited diffusion depth of Zn vapor into alumina. Note that a multilayer of ZAO/$Zn_4Al_{22}O_{37}$/ZnO was observed on the surfaces of the template. The thin (<4 nm) layer of a Zn-deficient phase $Zn_4Al_{22}O_{37}$ is a transition phase of the eventual ZAO. The existence of such multilayer supports that the reaction is diffusion limited and based on a bulk diffusion mechanism. Interestingly, after longer sintering (viz., >800 min at 660 °C), a ZnO nanonet can also be formed epitaxially on the ZAO nanonet surface. Such an epitaxial growth might explain the vertical alignment of ZnO nanowires we obtained using a ZAO covered sapphire as the substrate.

In Zhao's experiment, the Zn precursor was provided by [$Zn(TePh)_2$(tmeda)] solution which was infiltrated into the alumina pores.[35] After annealing in air for 24 h at 500 °C, nanowires of single-crystalline Te core surrounded by a polycrystalline ZAO shell were formed. It was suggested that the reaction underwent an intermediate phase of ZnTe which was then oxidized to ZnO plus elemental Te. Such freshly formed ZnO then reacted with the alumina pore wall to form the spinel. After removal of the Te core, ZAO nanotubes with a thin (8 nm) and polycrystalline wall were obtained (Fig. 3b).

We have demonstrated a different fabrication route to ZAO spinel nanotubes based on the Kirkendall effect (Fig. 4).[36,37] In this strategy, pre-synthesized ZnO nanowires (10–30 nm thick, up to 20 μm long) were coated with a 10 nm thick conformal layer of alumina *via* atomic layer deposition (ALD). Thus formed ZnO–Al_2O_3 core–shell nanowires were annealed in air at 700 °C for 3 h, causing an interfacial solid-state reaction and diffusion. Because the reaction is effectively a one-way transfer of ZnO into the alumina, it represents an extreme Kirkendall effect.[38] Upon a suitable matching of the thickness of the core and the shell, highly crystalline single-phase spinel nanotubes are obtained, as shown in Fig. 4a and b. Fig. 4b shows a TEM image of one nanotube together with the remaining gold particle atop the pristine ZnO nanowire. The spinel nanotube wall thickness can be precisely controlled through the variation of the alumina shell thickness *i.e.* the number of ALD cycles.

In addition, a suitable annealing temperature is very important. Fig. 4c displays how the morphology of the final product depends on the annealing temperature:[39] Tiny voids are generated at ZnO/Al_2O_3 interface near 600 °C, but do not grow to large voids due to kinetic reasons. Reaction at 700 °C results in good crystalline nanotubes as long as the thicknesses of the wires and shell are well matched. Interestingly, a higher annealing temperature near 800 °C results in hollow nanotubes even if the initial ZnO nanowire is thicker than necessary for a complete spinel formation of the former shell. This is an effect of reactive desorption, that the surface ZnO decomposes and evaporates in the presence of reactive Al_2O_3. However, when the temperature is further increased, the tube wall collapses driven by the thermodynamic instability. Therefore, the temperature window for an optimal solid-state reaction of the core/shell nanowires is 700–800 °C.

The conformity and uniformity characteristics of ALD are essential to the formation of smooth nanotubes. Particularly, the synthesis of complex tubular ZAO nanostructures by such a shape-preserving transformation is possible if one starts with

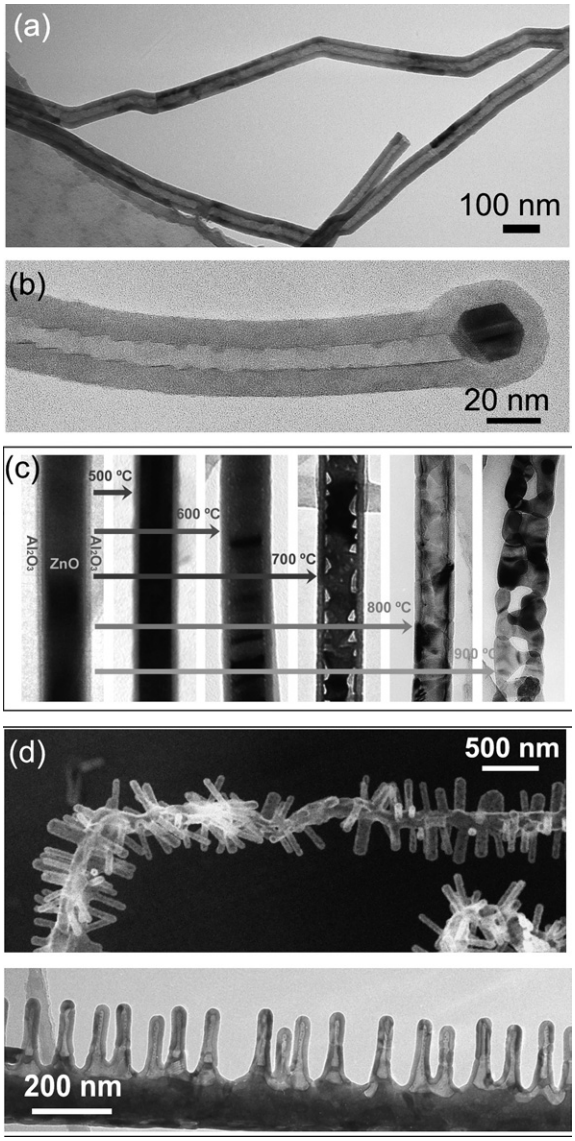

Fig. 4 $ZnAl_2O_4$ tubular nanostructures by solid-state reaction of ZnO/Al_2O_3 core/shell nanowires. (a–b) TEM images of straight nanotubes. Reprinted with permission.[36] (c) Effect of the annealing temperature to the morphology. Reprinted with permission.[39] Copyright 2008 American Chemical Society. (d) Complex tubular structures using hierarchical ZnO nanowires as the starting material. Reprinted with permission.[40] Copyright 2008 American Chemical Society.

hierarchical 3-D ZnO nanowires.[40] Recent literature shows an abundant variety of ZnO 3-D nanostructures including bridges, nails, springs, and stars (the readers can refer to the reviews in ref. 3–12). Fig. 4d give two examples: a Chinese firecracker-like 3-D and a comb-like 2-D hollow nanostructure ZAO spinel. Such uniform structured products cannot be obtained by other coating methods like pulsed laser deposition, sputtering or physical vapor deposition because their directionality causes shadowing and poor step coverage.

Because of the above mentioned reaction, we expect that the ZnO nanowires grown inside porous alumina templates (especially those by Zn electrodeposition plus post-oxidation)[41–43] are not pure ZnO, but a mixture of ZnO with a layer of ZAO or

$Zn_4Al_{22}O_{37}$, since their growth or annealing temperatures were high enough for the spinel-forming solid-state reaction to occur. Unfortunately none of these papers have shown a high-resolution TEM of the nanowires. Likewise, the growth of ZnO nanowires directly on the lattice-matched sapphire (single crystal Al_2O_3) might also end up with formation of ZAO spinel, as pointed out recently by Grabowska *et al.*[44]

Contribution of surface diffusion. Previous discussions on Kirkendall-type diffusions consider a continuous bulk diffusion of the growth species and vacancies. Therefore, the pore enlarges only by aggregation of inward-flux excess vacancies at the centre of the core. However, in most real experiments especially nanoscale objects, voids are generated near the interface and separate the core from the inner surface of the product layer. In this case, bulk like diffusion is limited and the above formulated diffusion considerations become invalid. We have proposed a conceptual extension based on our experimental observations,[45] suggesting main stages to be involved in the development of the hollow interior. The initial stage is the generation of small Kirkendall voids *via* a bulk diffusion process intersecting the product interface. These voids should have a fairly uniform size distribution. The second stage is dominated by surface diffusion of the core material (viz., the fast-diffusing species) along the pore surface. As surface diffusion coefficients are normally several orders of magnitude larger than their bulk counterparts, a faster kinetics of the void growth is expected. Such surface diffusion-assisted growth would make the voids less spherical and their size distribution larger as evident in our experiments. Fig. 5 gives examples of Kirkendall voids developed at different stages. In this case, the ZnO core with a diameter of around 65 nm was thicker than necessary for a shell consuming spinel reaction. The observation of small voids of equal size at the interface after the low-temperature (600 °C) annealing indicates homogeneous nucleation and growth of Kirkendall voids. After annealing at 700 °C, the voids grow and become irregular in shape and size, clearly illustrating the contribution of surface diffusion at a later stage.

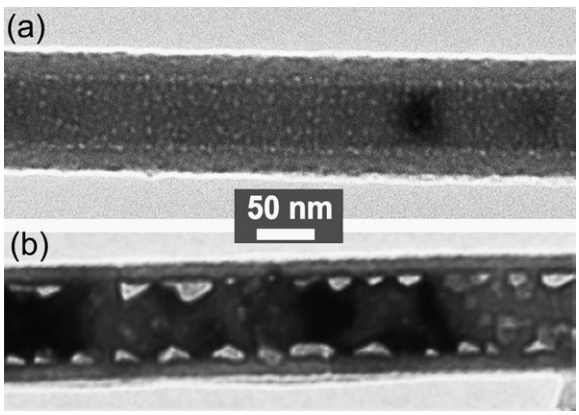

Fig. 5 Supporting evidence for the influence of surface diffusion on the morphology evolution during annealing of ZnO/Al_2O_3 core/shell nanowires. (a) Defocused TEM image of a nanowire annealed at 600 °C for 15 h. The initial voids are tiny and uniform in size. The voids are distributed near the interface but not within the Al_2O_3 layer, indicative of their nature of Kirkendall voids, rather than voids caused by crystallization of the amorphous alumina. (b) TEM image of a sample annealed at 700 °C for 5 h, showing the increase in the void size and shape inhomogeneity.

$ZnGa_2O_4$

Zinc gallate (ZGO) is probably the most studied among all spinel nanostructures, because of its interesting luminescent properties. It is a promising candidate for a blue light source (based on electroluminescence), for vacuum fluorescent displays (based on cathodoluminescence)[46] and for gas sensing (based on surface state-related electric properties). ZGO has a wide bandgap of 4.4 eV, thus is transparent from the violet to the near ultraviolet region. There is a self-activated blue (430 nm) emission stemming from the tetrahedral Ga–O groups in the spinel lattice (meaning that Ga not only occupies octahedral sites but also some tetrahedral sites when a Ga-rich sample is prepared).[47,48] Furthermore, it is proposed that ZGO can be a host for full color emitting materials when doped with various activators: Mn^{2+} for green[49] and Eu^{3+} or Cr^{3+} for red.[50] Traditional solid-state reaction of Ga_2O_3 and ZnO powders at 1000–1300 °C has been applied to prepare ZGO ceramics or sputtering targets.

The demonstrated fabrication routes of 1-D ZGO nanostructures can be divided into two main categories. First, high-temperature (around 1000 °C) co-evaporation of a mixture of ZnO–Ga powders and deposition substrates. The growth is driven by the well-known vapor-liquid-solid mechanism with gold nanoparticles acting as the catalyst. One drawback of this method is the difficulty of controlling the Ga/Zn ratio so that a ZnO phase might co-exist with the ZGO spinel even if the source material is mixed with a defined molar ratio. Nevertheless, Bae *et al.*[51] fabricated pure cubic phase spinel nanowires vertically standing on a Si substrate using a gold nanoparticle catalyst for the vapor-liquid-solid growth by employing this method. All the nanowires grow along the [111] direction. Using the same technique, Feng *et al.*[52] obtained ultralong nanowires on an Au covered Si substrate which were mainly ZGO but with a small amount of ZnO. A particularly interesting discovery was the helical ZGO nanowires wrapped around straight ZnSe nanowire supports, as well as free-standing ZGO nanowires self-coiled into spring-like structures (see Fig. 6a).[53] These zigzag wires elongate periodically along the four equivalent <011> directions, with an oblique angle of 45° (so as to maintain a coherent lattice at the kinks). According to the authors,[53] this unique growth behavior might be, related to the ZnSe nanowires, which provide the Zn source at the beginning and simultaneously an epitaxial substrate for ZGO. Note that the evaporation temperature used by the authors was as low as 600 °C.

The second type of fabrication route is a two-step process: synthesis of single-crystalline nanowires followed by their reaction with the other oxide. The latter step is a typical solid-state reaction on the nano scale, which results in an outer ZGO layer surrounding the nanowire core. Pure ZGO spinel can be obtained by dissolving the remaining core material. The spinel nanoshell or nanotubes can be single crystalline as a result of the epitaxial relationship between the growing ZGO and the core material. Chang and Wu[54] made a systematic study of the formation of ZGO layer on top of β-Ga_2O_3 nanowires. Nanowires of a single-crystalline Ga_2O_3 core and a CVD-grown

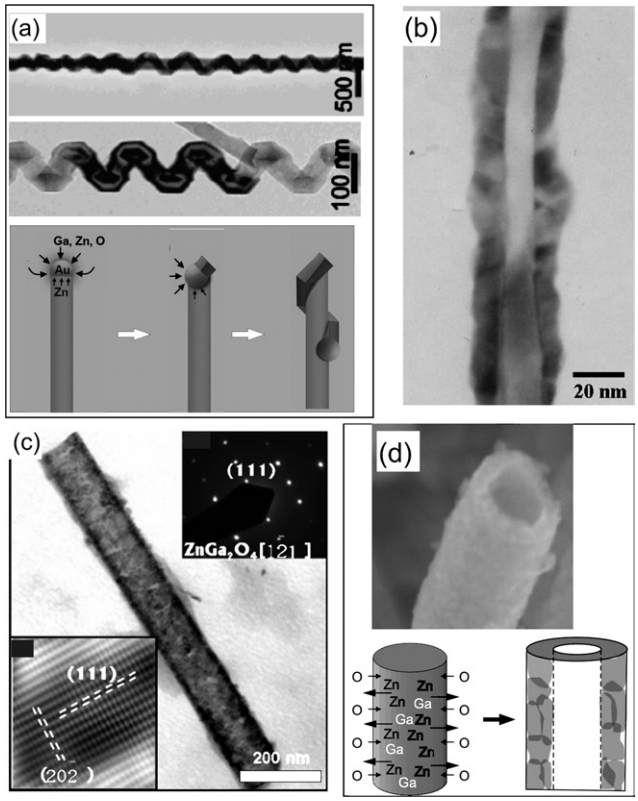

Fig. 6 $ZnGa_2O_4$. (a) Nanovines of a helical $ZnGa_2O_4$ nanowire swirling around a straight ZnSe nanowire (top) and a spring-like nanowire without the ZnSe support (middle), and the proposed formation mechanism (bottom). Reprinted with permission.[53] Copyright 2006 American Chemical Society. (b) $ZnGa_2O_4$ nanoshell with a Ga_2O_3 core by solid-state reaction of the Ga_2O_3/ZnO core/shell nanowires. Reprinted with permission.[54] Copyright 2006 American Chemical Society. (c) $ZnGa_2O_4$ nanotubes by reaction of initial ZnO nanowire with Ga–O vapor and removal of the remaining ZnO core. Insets are the corresponding electron diffraction pattern and high-resolution TEM image showing the single-crystallinity of the nanotube. Reprinted with permission.[55] © 2006 American Institute of Physics. (d) $ZnGa_2O_4$–ZnO compound nanotubes and the proposed formation mechanism which involves a faster outward diffusion of Zn/Ga than the inward diffusion of O. Copyright Wiley-VCH Verlag GmbH & Co. KGaA. Reprinted with permission.[56]

polycrystalline ZnO shell were annealed at 1000 °C for 1 hr. Depending on the thickness of the ZnO layer, the final product after the solid-state reaction was either Ga_2O_3/ZGO core–shell nanowires, ZGO nanowires, or ZGO nanowires capped with ZnO nanocrystals. In any cases, the ZGO were single crystalline. An epitaxial relationship was identified as ZGO[040] || Ga_2O_3[003]; ZGO[111] || Ga_2O_3 [$\bar{2}$01]. Fig. 6b shows an example of the Ga_2O_3 core/ZGO shell nanowire.

Li *et al.*[55] did a similar experiment but in the opposite way: they started with ZnO nanowire array, which reacted *in-situ* at 500 °C with a Ga_xO_y surface layer deposited from the vapor, forming a ZGO spinel layer. Because of the epitaxial interface, ZnO [1$\bar{1}$0] || ZGO [11$\bar{2}$]; ZnO [110]|| ZGO [4$\bar{4}$0], the ZGO layer as well as the subsequent ZGO nanotubes were single crystalline. Fig. 6c shows the nanotubes together with the electron diffraction pattern which proves its single crystallinity. Hereby, the phase was controlled by the deposition temperature, unlike Chang and Wu's case where the phase was controlled by the shell thickness.

Another special way to obtain ZGO spinel nanotubes was reported in Tsukuba.[56] Ga-doped ZnS nanowires were heated in an oxygen gas flow at 500–850 °C for 200 min, which converted the Ga:ZnS nanowires into nanotubes whose walls are comprised of ZnO + ZGO composite fragments. A low-magnification SEM image of these nanotubes is shown in Fig. 6d. While the overall 1-D structure and morphological homogeneity of the initial nanowire were preserved after the reaction, the nanotube wall became polycrystalline and rugged. A possible formation mechanism involves unequal diffusion rates for the outward Ga/Zn and inward oxygen during the oxidation of the ZnS nanowires: the former higher than the latter so as to produce a hollow interior along the length (Fig. 6d). This is similar to the Kirkendall effect in the case of the ZnO + Al_2O_3 reaction.[36,37] As the Ga concentration in the initial ZnS nanowires is only on the doping level, it is not surprising that the nanotube walls are not pure ZGO. Annealing of a Ga-doped ZnO nanowire will certainly not give similar nanotubes as above.

All the so-far demonstrated ZGO nanowires or nanotubes are undoped, so the observed emissions in their luminescence spectra are related mainly to the self-activated Ga–O emission or composition stoichiometry (*e.g.*, O vacancies, Zn interstitials). Two main peaks commonly have been observed: one near 380 nm and the other near 430 nm. But there seems little point comparing data from different authors since the peak position is highly sensitive to the preparation conditions and can shift by more than 200 nm depending on the Zn/Ga stoichiometry. For applications in nanoscale light sources, doping with rare-earth elements into the 1-D ZGO nanostructures is needed.

Zn_2TiO_4

Zinc titanate is a useful material for low-temperature sintering dielectrics. Usually, there are three modifications for the ZnO–TiO_2 system: Zn_2TiO_4 (cubic), $ZnTiO_3$ (hexagonal) and $Zn_2Ti_3O_8$ (cubic). Zn_2TiO_4 (ZTiO) is known to have an inverse spinel crystal structure: half of the Zn are at tetrahedral interstices and the remainder sharing octahedral interstices with Ti ions. ZTiO has been widely used as a regenerable catalyst as well as an important pigment in industry. It is also a good sorbent for removing sulfur-related compounds at high temperatures. Since nanoscale ZTiO is expected to achieve low-temperature sintering—a desirable property for microwave dielectrics—increasing attention has been paid to the preparation of ZTiO in a nanoscale form in recent years.

Conventional synthesis methods such as high-energy ball milling and a high-temperature solid reaction have been reported to prepare ZTiO nanocrystallites. For example, nanocrystalline ZTiO spinel can be prepared easily by high-energy ball milling a stoichiometric (2:1) mixture of ZnO and α-TiO_2 at room temperature.[57] However, the reports on 1-D ZTiO nanostructure growth are scarce. Only recently, Yang *et al.*[58] reported the synthesis of twinned ZTiO nanowires by using ZnO nanowires as a reactive template. In the experiments, ZnO nanowires with an axis direction along [01$\bar{1}$0] were coated with amorphous Ti by magnetron sputter deposition to form ZnO/Ti core/shell

nanowires. Since the atomic ratio of Ti/Zn for forming stoichiometric ZTiO was supposed to be 1:2, the sputtering conditions were optimized to yield a maximum quantity of nanowires, viz., 30–40 nm thick Ti shell for 40–60 nm thick ZnO core. After thermal annealing at 800 °C for 8 h at low vacuum, the solid-state reaction led to a phase transformation from wurtzite ZnO to ZTiO. The final product contained a large amount of (111)-twinned ZTiO nanowires elongated along the [111] direction. Structurally the sputter-deposited Ti layer was not conformal. Moreover, the electron and ion bombardment also causes content fluctuation in the ZnO nanowires prior to the solid–solid reaction. It was discussed that these two types of non-uniformity contributed to the formation of ZnTiO subcrystallites, eventually causing the zigzag morphology of the nanowires.

We very recently synthesized 1-D twinned ZTiO nanowires *via* a solid-state reaction approach using ZnO nanowires as the template.[59] Different from above, a very thin (5 nm) layer of TiO_2 was deposited *via* ALD. Note that our ZnO nanowires, grown also by a gold-catalyzed vapor-phase route, were elongated along the [0001] direction. The TiO_2 layer was amorphous and surrounded the ZnO nanowires with a very uniform thickness. The ZnO/TiO_2 core/shell nanowires transformed into a zigzag structure, too, after annealing at 900 °C for 4 h in an open furnace (see TEM images in Fig. 7a and b). The twinned nanowire is composed of large parallelogram-shaped subcrystallites, but does not present periodic stacking (Fig. 7b). The interplanar spacings of 0.49 nm measured from the high-resolution TEM image perfectly match the d_{111} lattice distance of ZTiO crystals, demonstrating the [111]-oriented growth direction of each individual grain. The fast Fourier transform (FFT) pattern of the twin boundary (TB) (inset of Fig. 7c) reveals clearly the (111) twin structure: two $(1\bar{1}1)$ mirror planes sharing a common (111) face. The twinning angle across the boundary is measured to be about 141°, and the relative rotational angle is about 70.5° (Fig. 7c and d). These results are in agreement with other cubic nanowires like SiC, InP, and Zn_2SnO_4 (see also below). No misfit dislocations were observed at the interface.

It is proposed that the formation of twinned ZTiO nanowires in our case includes multiple stages, which differs from the one by Yang *et al.*[58] Since amorphous TiO_2 easily crystallizes at a temperature of 300 °C or higher, the initially continuous TiO_2 shell on the surface of ZnO nanowires is expected to transform into anatase TiO_2 islands first. The islands are textured as a result of volume shrinkage of the amorphous phase. During the annealing at 900 °C, the TiO_2 phase could be incorporated in the ZnO lattice as segregation at early stages because of the faster diffusion speed of Ti^{4+} than that of Zn^{2+}. Subsequently, ZTiO spinel nanocrystallites formed through lattice rearrangement and were attached to the surface of the unconsumed ZnO core (note that the TiO_2 layer was only 5 nm thick). No voids or tubular structures appeared at the ZTiO/ZnO interface, indicating that the inner diffusion of Ti^{4+} is prominent for the TiO_2/ZnO couple. With prolonged annealing at 900 °C, the unconsumed ZnO core is desorbed or evaporated at 900 °C through the gaps of the nanocrystallites. Subsequently, the loosely-interconnected nanocrystallites were [111]-orient attached, coalesced, and finally evolved into twinned nanowires seen in Fig. 7b.

By comparing the above two solid-state reaction experiments,[58,59] we are able to draw the following conclusions. First, the preferred [111] growth direction of the twinned ZTiO nanowires is independent of the orientation of the starting ZnO nanowires ([01$\bar{1}$0]or [0001]). During sintering, individual ZTiO nanocrystallites may rotate to constitute an energetically favorable assembly along the [111] direction, since the surface energy of [111] facets is the lowest for an fcc structure. Secondly, the diffusion species in ZnO/TiO_2 couple is unambiguously Ti^{4+}, not metallic Ti as described in the case of the ZnO/Ti couple. Last, fluctuation of the ZnO content is not necessary to form the subcrystallites.

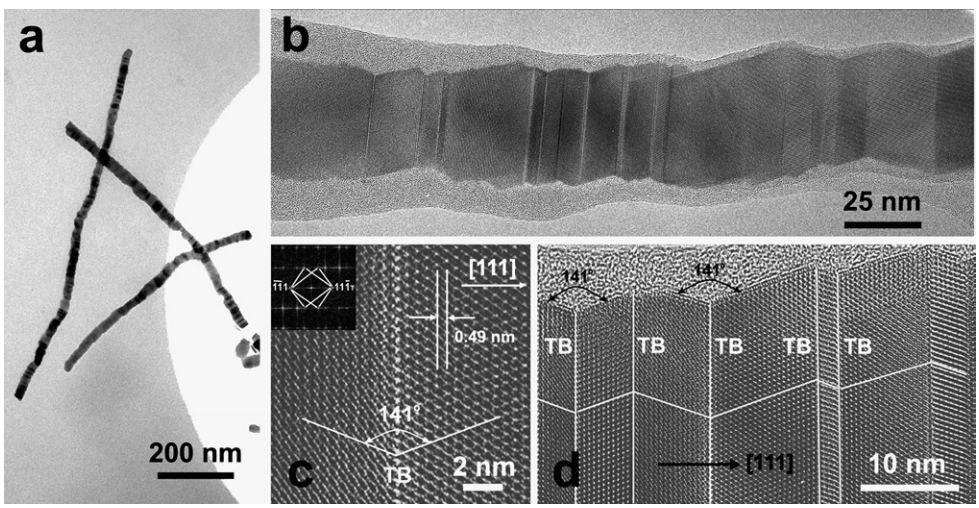

Fig. 7 Zn_2TiO_4 zigzag twinned nanowires by solid-state reaction of ZnO/TiO_2 core/shell nanowires. A uniform shell of TiO_2 was coated using atomic layer deposition and annealing conditions of 900 °C, 4 h. (a–b) TEM images at different magnification showing the zigzag morphology of the nanowires. Note that the twinning is non-periodic. (c) A closer view of one twin boundary and the corresponding FFT pattern. (d) Several twinning boundaries with a fixed zigzag angle of 141°. Yang *et al.*, unpublished work.

Zn_2SnO_4 and twinning

As in the case of Zn_2TiO_4, Zn_2SnO_4 (ZTO) crystals also have an inverse spinel structure. The interest in ZTO is for its use in electrical circuits as a transparent conducting electrode replacing the expensive ITO (In-doped SnO_2). This is because of its high electron mobility, high electrical conductivity, and low visible absorption. Like other metal-oxide semiconductors, ZTO can also have potential applications in photovoltaic devices and Li-ion batteries.[60,61] While ZTO nanoparticles have been demonstrated to be useful as electrodes of dye-sensitized solar cells (*e.g.*, light-to-electricity efficiency of 3.8%),[61] it is envisaged that 1-D nanostructures could enhance the performance due to a continuous electrical conduction path.

1-D ZTO nanostructures are fabricated mainly by thermal evaporation of a powder mixture of ZnO + SnO_2 or Zn + Sn metal (and some by hydrothermal reaction). No report so far on solid-state reaction of core/shell nanowires has been published, although controlled growth of ZnO and SnO_2 nanowires has been become routine in many research labs. The high-temperature evaporation and deposition method involves a complicated thermodynamic and kinetic process. The partial pressures of oxygen and ZnO/SnO vapor are very inhomogeneous which causes disturbances of the Au–Zn–Sn ternary droplet size in the VLS growth and hence diameter oscillations.[62] Moreover, such an evaporation method usually ends up with a mixture of different phases and structures in one growth set. For example, ZnO, ZTO nanowires, and chainlike ZTO nanowires were identified in a single VLS growth.[62] The ZTO composition was off stoichoimetric with an element ratio of Zn:Sn:O = 1.75:1:(2.6–3.5), indicating a deficiency of zinc and oxygen. Reports on a series of ZTO nanostructures with very different morphologies have been published by the Xie group, who conducted similar evaporation experiments.[63–66] The so-far demonstrated ZTO quasi-1-D nanostructures are listed in Table 1, including smooth belts,[65,67] rings,[65] chainlike single-crystal wires,[63,66,68] twinned wires,[63,64,66,69] and short rods.[70] In the following we selectively discuss only two types of rather extraordinary nanostructures.

The first is the twinned nanowire (see Fig. 8a). These 1-D ZTO nanostructures have a twinning morphology similar to that of the aforementioned Zn_2TiO_4. Wang *et al.*[63,65,66] reported VLS-grown twinned ZTO nanowires by evaporating powder mixtures at 1000 °C with two types of weight ratios. In one case a ratio of ZnO:SnO = 2:1 gave twinned nanowires (among many other shaped wires), whereas in the other case, a ratio of ZnO:SnO = 1:4 was needed for the production of similar twinned wires. All these ZTO wires have a $[1\bar{1}1]$ growth direction, with the twin planes being $(1\bar{1}1)$ and the twinning direction perpendicular to the wire axes, same as observed for ZTiO nanowires.

The second is the single-crystal chainlike nanowire (see Fig. 8b). Structurally this type of wire is formed by a sequential stacking of rhombohedral nanocrystals along the $[1\bar{1}1]$ direction. The stacked nanocrystals constitute a single-crystal wire on the whole, as revealed by the electron diffraction pattern (*e.g.*, bottom of Fig. 8b). This means lattice coherence at the boundary of the nanocrystals. Jie *et al.*[62] observed so-called diameter-modulated ZTO nanowires composed of linked ellipses. Wang *et al.*[67] reported diamond-like wires composed of intersected

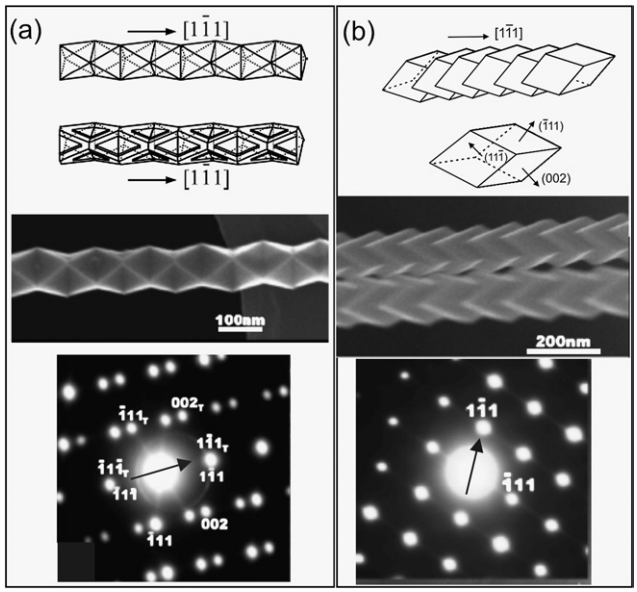

Fig. 8 Zn_2SnO_4. (a) Pseudoperiodic twinned nanowire. (b) Single-crystal nanowires produced by periodic stacking of rhombohedral nanocrystals. Top: schematics of the structures; middle: SEM images; bottom: the corresponding electron diffraction patterns. The arrows in the diffraction patterns indicate the nanowire growth directions. Reprinted with permission.[66] Copyright 2008 American Chemical Society.

rhombohedra (Fig. 8b). But according to the careful electron tomography study by Kim *et al.*,[68] who also obtained both types of chainlike ZTO nanowires, the above two structures actually are the same; the observed zigzag angles appear different (125° or 120°) under the electron microscope simply because of a rotation of the wire around its axis (see Fig. 5 of ref. 68).

Hydrothermal synthesis as a low-cost, high-yield method for 1-D nanostructures has been applied to single-crystalline ternary compound nanowires like $BaTiO_3$ and $PbTiO_3$ which are important ferroelectric materials,[71–73] and recently to ZTO nanowires. A hydrothermal process was applied with the use of hydrazine hydrate as the alkaline mineralizer for the growth of ultrathin (2–4 nm in diameter) ZTO nanowires.[70] The optical bandgap was determined to be 3.87 eV by diffuse UV-vis reflectance measurements, which is a blueshift of 0.27 eV from bulk ZTO (3.6 eV), indicative of quantum confinement effects.

Discussion about twinning. Twinning as planar defects in nanowires is becoming a very interesting topic and is widely studied for cubic crystals including not only the above Zn_2TiO_4 and Zn_2SnO_4 but also binary compounds like GaAs, GaP, InP, ZnSe, and SiC.[74–81] These nanowires are formed either through solid-state reactions or metal-catalyzed unidirectional growth, and quasiperiodic twinnings have been observed intersecting the entire wire cross section. It is known that the (111) twinned crystals have a relative rotational angle of 70.5° and the zigzag angle between two twinning nanounits is about 141°. This is in accordance with all the so-far demonstrated nanowires of the cubic phase.

Fig. 9 schematically illustrates the two typical growth processes of twinned nanowires. The first (Fig. 9a) represents the

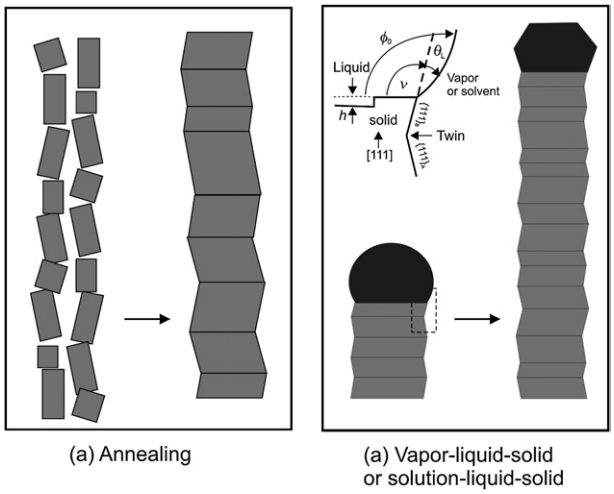

Fig. 9 Two main formation processes for twinned nanowires of cubic crystals. (a) Nanocrystallites are formed first through solid-state reactions, and then transformed into twinned nanowires during annealing. This process is mainly for ternary alloyed nanowires like Zn_2TiO4 and Zn_2SnO_4. (b) Twinned nanowires formed by vapor-liquid-solid or solution-liquid-solid growth processes. It is for both ternary compound spinel nanowires and binary nanowires like GaP, InP, GaAs, and ZnSe. Inset of (b) shows the three-phase boundary where a fluctuation in the droplet/nanowire contact angle causes nucleation of a twinned plane. Reprinted with permission.[78] Copyright 2007 American Chemical Society.

spinel nanowires grown by solid-state reactions, for example, the aforementioned Zn_2TiO_4 (Fig. 7). This is mainly a self-assembling process where subcrystallites rearrange to minimize the total energy: two adjacent (111) faces meet *via* a shear movement along the [21$\bar{1}$] direction of subcrystallites driven by dislocation-induced strain; and then mirror planes arrange symmetrically to reduce the total energy. Alternatively, the twinned structure can also be formed when new crystallites start to grow in a limited space between two existing grains *via* an Ostwald ripening process during the sintering stage.

In the second route (Fig. 9b), the nanowires grow through a VLS or solution-liquid-solid process with a ternary-alloy droplet at the growth front as the catalyst. The ZTO twinned nanowires (Fig. 8) and most of the binary compound zinc blende nanowires[74–81] fall into this category. In this case the formation of twins is strongly related to contact angle fluctuation at the three-phase boundary (inset of Fig. 9b), as elaborated by Davidson *et al.*[78] A smooth untwinned nanowire has (112) sidewall faces. But twinning eliminates the (112) sidewall surface by converting it to two lower energy (111) mirror planes. The sidewall surface alternates between the two (111) mirror planes with subsequent twins in order to maintain straight nanowire growth along the [111] direction. In the Davidson model, fluctuations in the droplet/nanowire contact angle for Au-seeded nanowires are most likely necessary for twinning to occur. This requirement (contact angle at the three-phase boundary must fluctuate sufficiently) indicates that even when twin planes might be expected based on their formation in bulk crystals, they may not form in nanowires. Interestingly, this model also suggests that a nanowire with a smaller diameter (<10 nm) exhibits less twinning because of the higher tendency to exhibit the lowest energy (111) and (110) planes.

$ZnFe_2O_4$

Nanostructured ferrite spinels are of special interest because of their size- and morphology-related magnetic properties. While most ferrite spinels have inverse spinel structures and are ferrimagnetic, $ZnFe_2O_4$ (ZFO) has a normal spinel structure and shows long-range antiferromagnetic ordering at its equilibrium state below the Néel temperature $T_N \approx 9$–11 K.[82,83] At room temperature, it is paramagnetic because of the weak magnetic exchange interaction of the B site Fe^{3+} ions. Nanoscale ZFO, however, can have a higher T_N, or show ferromagnetism with the magnetization generally increasing with grain size reduction. There are a number of reasons for this feature, such as inversion of the cation distribution (Fe^{3+} into tetrahedral interstices and Zn^{2+} into octahedral interstices), small size effect (a large surface area gives uncompensated magnetization moment), and non-stoichiometry.[84–87] For example, the ZFO nanoparticles with diameters of $\approx$10 nm have shown a saturated magnetization of $M_s = 44.9$ emu/g at room temperature.[87] The magnetic behavior of the nanocrystals was related to the ferromagnetic coupling of Fe ions at A–B sites in the $(Zn_{1-x}Fe_x)[Zn_xFe_{2-x}]O_4$ particles and surface spin canting.

While there are quite a number of reports on ZFO nanoparticles, there are strangely only a few publications on ZFO nanotubes or wires. Jung *et al.*[88] fabricated ZFO nanowires by annealing the densely packed ZFO nanoparticles infiltrated into porous alumina templates (see Fig. 10a). The nanowires are

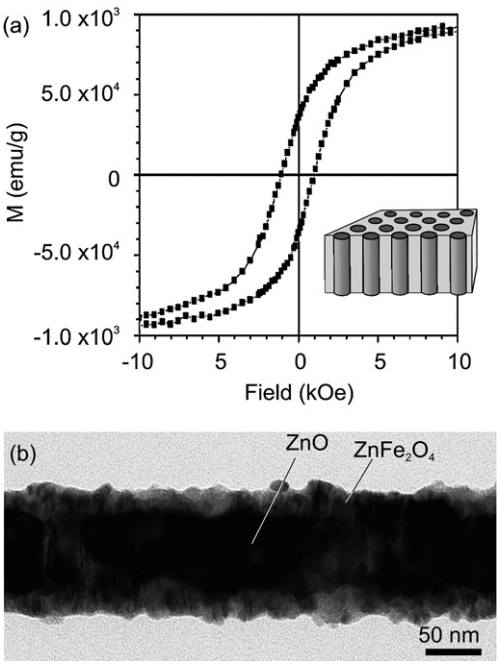

Fig. 10 Zn_2FeO_4. (a) M–H hysteretic loop of nanowires embedded inside porous alumina template. Inset is a schematic of the sample. Reprinted with permission.[88] © 2005 IEEE. (b) TEM image of $ZnFe_2O_4$ nanoshell with a ZnO core, obtained by annealing ZnO/Fe_2O_3 core/shell nanowires at 800 °C for 4 hr.

superparamagnetic and show evident increase in the coercive field and M_r/M_s value compared to the unannealed nanoparticles. Liu *et al.*[89] adopted a strategy similar to the standard solution synthesis of perovskite nanotubes/wires:[90] $Zn(NO_3)_2 \cdot 6H_2O$ and $Fe(NO_3)_3 \cdot 9H_2O$ with 1:2 molar ratio of Zn/Fe were dissolved into the mesopores of a silica SBA-15 template. After drying, decomposition and annealing, polycrystalline ZFO nanowire bundles were obtained, which also show enhanced paramagnetism compared to the bulk phase.

Different from the above negative template methods, ZFO nanoshells using ZnO nanowires as the template were prepared. Single-crystalline ZnO nanowires were coated with a uniform amorphous layer of ALD Fe_2O_3 using $Fe_2(O^tBu)_6$ precursor.[91] After annealing the core–shell nanowires at 800 °C for 4 h, an outer layer of ZFO surrounding the remaining ZnO was formed. An example of the obtained structure is shown in Fig. 10b where the initial ALD Fe_2O_3 is 20 nm thick. It is expected that the solid-state reaction of ZnO–Fe_2O_3 occurs by a Wagner counter-difussion mechanism. Unlike the ZnO–Al_2O_3 which is characterized by very smooth inner surface of the nanoshells, the interface after the solid-state reaction is rugged although the ZFO layer is single-crystalline (Fig. 10b). The crystallinity can be attributed to an orientation relationship $ZnFe_2O_4(111)$ [110]// ZnO(0001) [11$\bar{2}$0], as established by Zhou *et al.*[92] Since these nanoshells have a large aspect ratio of up to 100 and tunable shell thickness on an atomic scale, it would be interesting to examine their anisotropy magnetic properties. Systematic characterization is still under way.

Another related magnetic spinel is the recently reported $ZnCo_2O_4$ in the form of nanocubes due to the nanoscale Kirkendall effect.[93]

$ZnCr_2O_4$

After submission of this Feature article, an interesting publication[94] appeared reporting the conversion of elemental metal nanowires into the corresponding nanotubes, among which is the spinel $ZnCr_2O_4$. The reaction is an unconventional solid-vapor type: solid Zn nanowires reacted with CrO_2Cl_2 vapor in an oxygen environment at 400 °C for 3 h in a resistance furnace. The nanotube walls are granular and polycrystalline and possibly contain pores; nevertheless the XRD spectrum does correspond to a cubic, normal spinel-type structure. Note that the reaction temperature was much lower than ≥900 °C used for conventional solid-solid reaction of ZnO–Cr_2O_3 powder mixtures. As learned from properties of bulk or thin films, it would be of wide interest to investigate the antiferromagnetic ordering ($T_N \approx 12$ K)[95] and gas-sensing properties[96] of $ZnCr_2O_4$ nanotubes.

Zn_2SiO_4

Zinc silicate (ZSO), normally referred as mineral willemite, is the zero-pressure phases among many other high-pressure phases.[97] ZSO does not belong to the normal spinel group, because the ionic radius ratio of Zn^{2+} (0.074 nm) to Si^{4+} (0.041 nm) is too large to be stabilized in the cubic spinel structure. In mineralogy, ZSO synthesized at ambient pressure is expected to have a rhombohedral crystal structure with lattice constants close to a = b = 1.3938 nm and c = 0.9310 nm (JCPDS Card: 08-0492 or 37-1485). However, the phases of synthetic 1-D ZSO nanostructures appear to be inconsistent: rhombohedral,[98] orthorhombic[99,100] and tetragonal[101] phases have been claimed. ZSO emits typically green light at around 520 nm.

There are so far three publications available for 1-D ZSO nanostructures. The Wang group reacted ZnO nanowires either *in-situ* with Si vapors sublimated from the Si substrate,[99] or *ex-situ* with a CVD-deposited Si outer layer (*i.e.*, ZnO/Si core/sell nanowires).[100] In the former solid-vapor reactions at ≈600 °C, a porous ZSO nanosheath wrapping around the remaining ZnO nanowires was formed (Fig. 11a–b). In the latter solid-solid reaction at 900 °C, tubular segments were formed as a result of the continuity of the outer Si layer (Fig. 11c). In both experiments, the ZSO nanosheath is single-crystalline due to an orientation relationship at the interface. Regarding the growth mechanism, the authors suggested that physical evaporation of ZnO (600–900 °C) was the origin of the pores and hollow interiors. This is to be ascertained as we found that the evaporation of ZnO nanowires at 800 °C at a vacuum of 10^{-5} mbar is insignificant (no evident change of surface morphology). It could be that this reaction is the same as that for ZnO–Al_2O_3,[36] or it involves an enhanced desorption of ZnO catalyzed by the solid-state reaction. The latter process has been supported by the

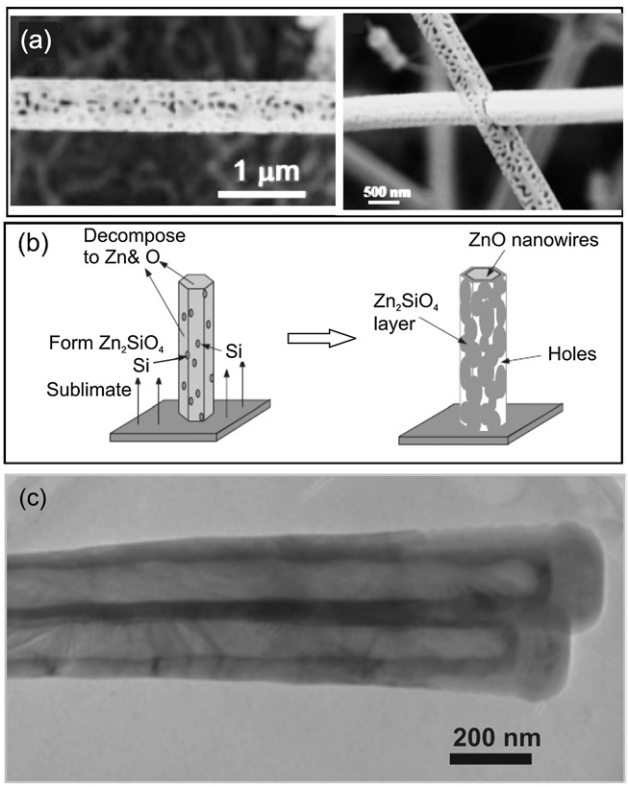

Fig. 11 Zn_2SiO_4 obtained by reacting ZnO nanowires with Si. (a) Porous nanosheath with a solid ZnO nanowire core, and (b) the corresponding schematic of the proposed formation process, which was an in-situ decomposition of ZnO nanowires and solid-vapor reaction at 600 °C with Si sublimed from the Si substrate. Reprinted with permission.[99] (c) A Zn_2SiO_4 nanotube as part of a tube-wire heterojunction by solid-solid reaction of ZnO/Si core/shell nanowires at 800–900 °C. Reprinted with permission.[100] Copyright Wiley-VCH Verlag GmbH & Co. KGaA.

$ZnO–Al_2O_3$ (ref. 102) and $ZnO–TiO_2$ spinel reactions[59] conducted in our group: in the presence of reactants on the nanowire surfaces, the ZnO decomposes more noticeably and the surface roughens until the total loss of the nanowire material upon extended annealing. Nevertheless, more uniform-structured ZTO tubes can be potentially obtained by using ALD SiO_2.

A hydrothermal method was applied by Xiong *et al.*[98] towards ordered Mn-doped ZSO nanowires (diameter 7–10 nm) using mesoporous silica SBA-15 as template. ZSO nanocrystals nucleated initially at the pore openings of the template. Further hydrothermal growth from the seeds was constrained to be 1-D elongation by the surfactant P123. Remarkably, these nanowires are single crystalline, similar to most hydrothermal-grown ZnO nanorods but unlike the polycrystalline ZAO nanotubes formed inside the anodized alumina channels.[35] Room-temperature photoluminescence spectra showed a characteristic green emission near 524 nm for different Mn-doping levels.

Such interfacial reaction should be concerned for device application of the ZnO/Si system. For example, Xu *et al.*[101] studied the atomic diffusion between a sputtered ZnO film and Si substrate, and found that a ZSO layer formed within ZnO. Coming to the nano-scale, it is reasonable to imagine that those popular high-temperature vapor-phase growths of ZnO nanowires directly on Si substrates may actually end up with a transition layer of ZSO. This might introduce artifacts when measuring the rectifying I–V curve of ZnO nanowires on top of *p*-type Si substrates. This issue has not been taken into account by the ZnO nanowire community, to our knowledge.

A similar system is Zn_2GeO_4 which also has a willemite (non-spinel) crystal structure. A very recent report by Tsai *et al.*[103] demonstrated the formation of single-crystalline Zn_2GeO_4 nanorods due to an agglomeration of Zn-containing Ge nanoparticles in water and subsequent aging. The nanorods were not in pure phase but together with amorphous membranes, which is an intermediate phase composed of Zn, Ge, and oxygen. These nanorods exhibit a blue-green luminescence peak at 450 nm.

ZnMgO

Alloying ZnO with MgO has been a promising way to widen the bandgap of ZnO-based nanowires while preserving the wurtzite lattice.[104–107] The alloyed $Zn_{1-x}Mg_xO$ crystal can maintain the wurtzite structure up to a Mg concentration of $x = 33\%$, with a bandgap of 3.99 eV.[108] Structurally, the nanowires are smooth if x is lower than 0.20. However, roughening was observed when the Mg concentration increased,[4,106] which caused the transition from a wurtzite to a rocksalt crystal structure.

We have attempted to synthesize ZnMgO alloyed nanowires using the CVD method inside a horizontal resistance furnace. Two experimental strategies were employed: first, two source materials, ZnO+graphite powder and Mg_3N_2 powder, were added in the same experiments and located at different temperature zones. In this case, the degree of alloying is very inhomogeneous as we observed nanowires of pure MgO, ZnO, ZnMgO, and ZnO–MgO longitudinal heterojunctions in a single experiment. This is most likely due to the inhomogeneity of the vapor concentration at the different regions of the substrate. The second strategy was that pre-grown ZnO nanowire arrays were subjected to Mg vapor at ca 780 °C for 45 min in the same growth chamber. The residual/leaky air provides oxygen to oxidize the Mg. The results are shown in Fig. 12a–b.

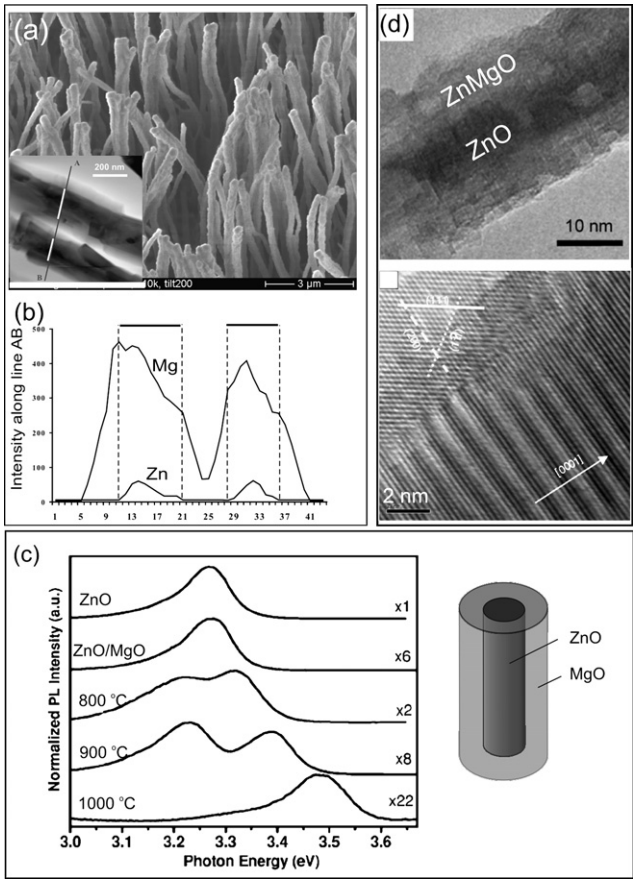

Fig. 12 ZnO/ZnMgO core/shell nanowires. (a–b) Heterostructure ZnO/ZnMgO core/shell nanowires by reacting ZnO nanowires with Mg vapor at ca 780 °C for 45 min. (a) The wires become curved compared to the original straight ZnO nanowires; (b) EDX spectrum recorded across two wires shown as inset in (a). The Zn peaks are aligned with, but narrower than, the Mg peaks, indicating the structure of a Zn-rich core and a Mg-rich shell. (c) Room-temperature photoluminescence spectra of ZnO/MgO core/shell nanowires and the wires after annealing at 800–1000 °C, showing the peak shift with increase of Mg concentration. Reprinted with permission.[106] © 2006 American Institute of Physics. (d) Radial heterostructured ZnO/ZnMgO nanowire grown in one step by molecular beam epitaxy. Top: difference in brightness intensity between core and sheath regions; bottom: an atomic-resolution view of the interface. The (Mg,Zn)O sheath is in the upper-left region and the ZnO core in the lower-right region. Reprinted with permission.[4]

The original smooth and well faceted ZnO nanowires were roughened and became curved. The curved shape could be partly due to stain at the core–shell interface, caused by their different lattice structures (ZnO: hexagonal, $a = 3.25$ Å, $c = 5.21$ Å; MgO: cubic, $a = 4.24$ Å). The shell is polycrystalline containing MgO grains with different orientations. TEM investigation of one of such core–shell nanowire with a large ZnO core thickness clearly shows the rough interface. Elemental mapping of two wires (Fig. 12b) indicates the structure of a ZnO core and a MgO shell. However, it is likely that a transition interface of ZnMgO alloy exists. A similar structure was revealed in the study by Hsu *et al.*[106] who conducted post-annealing of the ZnO/MgO

core/shell nanowires at 800–1000 °C. A continuous blue shift of the near bandgap luminescence emission was observed with annealing temperature, indicating the increase in Mg concentration in the alloyed ZnMgO nanowires (Fig. 12c). Fig. 12d shows a high-quality radial heterostructure nanowire with a ZnO core and rock salt ZnMgO sheath, grown in one step in MBE (molecular beam epitaxy).[4] These heterostructure nanowires may show quantum confinement effects.

Lorenz *et al.*[104] fabricated single-phase ZnMgO nanowires using PLD (pulsed laser deposition), in which the Mg concentration was varied in the range of 0–20% by changing the gas pressure. Fig. 13a gives a general view of the smooth ZnMgO nanowires; the morphology varies significantly at different substrate positions, which is a characteristic disadvantage of PLD. Cathodoluminescence of the nanowire arrays shows obviously the ZnMgO peak near 3.436 eV, relative to an undoped ZnO emission at 3.361 eV (Fig. 13b). The Mg concentration was then deduced from the emission energy to be $x = 0.046$ based on the estimation $E(Zn_{1-x}Mg_xO) = E(ZnO) + 1.64\,x$, where the E denotes the excitonic peak energy. The peak energies determined from different places of one sample exhibit only a small fluctuation as seen in Fig. 12b, indicative of a relatively uniform Mg concentration in the nanowires.

The quantum well structure of the ZnMgO–ZnO superlattice (narrow bandgap ZnO embedded within wide bandgap ZnMgO) is well established in films which are grown using MBE, and a quantum Halle effect has been observed by the Kawasaki group.[109] Promising results on nanowire $ZnO/Zn_{0.8}Mg_{0.2}O$ multi-quantum wells have also been reported,[110,111] and more recently by various groups.[112] This may lead to fundamental research on 1-D electron ballistic transport, and also applications in nanoscale LEDs (light-emitting diodes). Fabrication of a radial quantum well structure surrounding a pristine ZnO nanowire is a challenging but interesting avenue to explore.

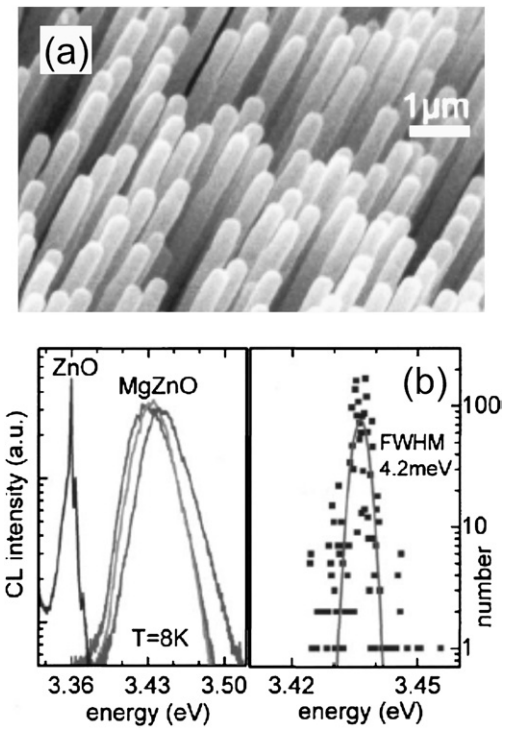

Fig. 13 Pure ZnMgO alloy nanowires grown by pulsed laser deposition. (a) General morphology of the wires. (b) Left: Three typical cathodoluminescence spectra recorded from one sample, together with a spectrum of a ZnO nanowire. Right: the histogram of peak energies with a Gaussian fit, indicating the relative uniformity in the Mg concentration in the alloy nanowires. Reprinted with permission.[104] © 2005 American Institute of Physics.

Applications

The main application potential of spinels, in the form of powders or thin films, includes catalysts, humidity and gas sensors, transparent conducting electrodes, battery anodes and light-emitting diode (phosphors). For those applications that rely on large surface areas and small dimensions, 1-D nanostructures are of interest and might be advantageous over powders. Nevertheless, there are so far few publications on the application of ZnO-based spinel nanowires and nanotubes. In the following, we discuss selectively two types of applications: gas sensors and Li-ion battery anodes.

Gas sensors

Because of the large surface-to-volume ratio and rich surface chemistry (charge transfer between nanowire surfaces and adsorbed molecules), most metal-oxide 1-D nanostructures exhibit electric properties sensitive to light illumination and ambient gas. Therefore, surface states play a major role in the optoelectronic properties. Optically driven oxygen and temperature sensing behavior of ZGO nanowires was recently demonstrated (see Fig. 14).[52] The current across individual nanowires was nearly zero at ambient conditions, whereas the forward-bias current increases drastically under illumination by 254 nm UV

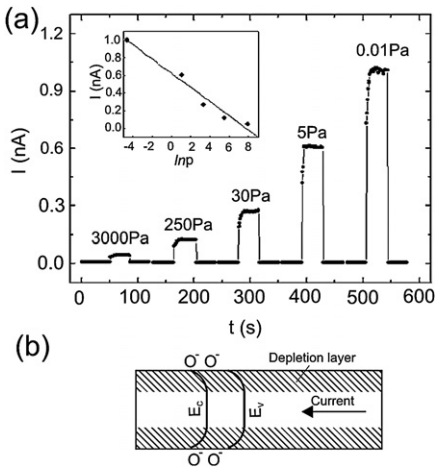

Fig. 14 Oxygen sensing of nanowires. (a) Forward-bias current across an individual $ZnGa_2O_4$ nanowire device (with Au electrodes) with UV light illumination at various O_2 gas pressures. The bias is 30 V and the temperature is 300 K. The inset is the current vs pressure curve, indicating a quasilogarithmic relation. Reprinted with permission.[52] © 2007 American Institute of Physics. (b) Band scheme of a nanowire showing the formation of a surface depletion layer due to oxygen adsorption. The depletion width depends on the surface coverage of the O^-.

light (the bandgap of ZGO is around 270 nm). Such a light response is illustrated by the spikes in Fig. 14. The response and recovery processes are faster (response time: ~2 s, recovery time: <1 s) than those of pure ZnO nanowires.[52] The enhancement in the forward current was attributed to the increased charge carrier concentration (*i.e.*, narrow or elimination of the oxygen-adsorption-induced surface depletion layer, see Fig. 14b) and decreased contact resistance (*i.e.*, lower the Schottky barrier height between the nanowire–Au contact). The current level is also dependent on the oxygen pressure (Fig. 14a), since a change in the pressure corresponds to a change in the oxygen adsorption rate. A similar pressure-dependent oxygen sensing behavior has been also observed in a $ZnSnO_3$ nanowire device.[113]

Li-ion battery anodes

ZnO itself is not a good anode material for Li-ion batteries, as it shows poor Li-electrochemical cyclability, resulting from volume variations during the alloying and de-alloying cycling. However, when it is compounded with its spinel derivative the performance can be improved. One example is given by Liu *et al.*[114] who investigated the electrochemical performance of a $ZnO/ZnAl_2O_4$ calcined layered-double hydroxide nanosystem as a Li-ion battery anode. The $ZnO/ZnAl_2O_4$ mixture system exhibited a first discharge capacity of 1275 $mAhg^{-1}$ and a discharge capacity of 500 $mAhg^{-1}$ after 10 cycles, together with improvement of the cycling stability as compared to pure ZnO. The improved electrochemical performance was ascribed to the $ZnAl_2O_4$ which is an inactive matrix and functions as a physical support to accommodate the larger lattice distortions of ZnO.

It has been shown by Sharma *et al.*[115] that the spinel nano-$ZnCo_2O_4$ (~20 nm) is an attractive material for evaluation as an anode for Li-ion batteries. Galvanostatic cycling at 25 °C (voltage range 0.005–3.0 V vs Li at 60 mAg^{-1}) gave reversible capacities of 900 mAh g^{-1}. Reasonably stable cycling performance was exhibited in the range 5–60 cycles with a ~98% coulombic efficiency. The reaction mechanism for Li-recyclability involves both de-alloying and alloying of Zn and displacement reactions, viz., LiZn ↔ Zn ↔ ZnO and Co ↔ CoO ↔ Co_3O_4. They showed that both Zn and Co ions act as mutual beneficial matrices, and the stable and high capacity is a result of a reversible capacity contribution of Zn through both alloy formation and displacement reactions. The electrochemical performance of $ZnCo_2O_4$ is comparable to that of Co_3O_4 (which is the most-studied metal-oxide anode material) and superior to that of commercial graphite.

Concluding remarks

The current research on ZnO-based ternary oxides remains still at a stage of fabrication and structural characterization. In terms of growth control, the thermal evaporation and deposition method is less effective than the solid-state reaction of the core/shell nanowire method. The latter is more directly related to the conventional solid-state reactions by reaction sintering so that the reaction kinetics and diffusion mechanisms can be more straightforwardly understood. Sputtering or CVD does not give homogeneous covering of high-aspect-ratio nanowires; ALD appears the best solution so far and most oxides can be processed by ALD, such as Al_2O_3, TiO_2, Fe_2O_3, In_2O_3, SnO_2, Cr_2O_3, SiO_2, as well as ZnO itself, so long as a suitable type of precursor is available.[116,117] Therefore the solid-state reaction method is transferable to a wide range of ZnO-based ternary compound nanomaterials.

Twinning and zigzag shapes (Fig. 8 and 10) are common phenomena for spinel nanowires, as a result of the equivalence of the crystallography planes and the associated energy. Similar twins can form from different growth processes (solid-state reactions, VLS growth) and/or different materials; the twinning mechanism also appears different but a universal mechanism might exist. Possibly, an in-situ reaction annealing experiment inside a TEM might provide valuable hints. Also, little is known about the electrical, mechanical, and in particular the light-emitting properties of these twinned nanostructures. Mechanical studies indicate that twin boundaries act commonly as dislocation obstacles to affect the deformation behavior of an fcc system. Hence, twins are expected to have an important influence on the electronic and mechanical properties.

Doping spinels with Er, Yb, Eu, Tb, Mn creates new luminescent centers, which then generally enhance the luminescence efficiency enabling tuning of the emission wavelength. Alloying two spinels improves carrier mobility which is beneficial for their applications in electrical contacts. While most of these studies are still in a traditional manner, *i.e.*, nanopowders and thin films, it could be a direction for future research efforts in spinel 1-D nanostructures. As most of the ZnO-based spinels are wide-bandgap semiconductors, nanowires could also find applications in flexible electronic displays, which is an emerging research topic.

Acknowledgements

We thank Dr R. Scholz, D. S. Kim, Dr M. Kenz, Prof. D. Hesse, Dr E. Pippel, and Prof. U. Gösele in Max Planck Institute of Microstructure Physics, Halle, for their helpful discussions.

References

1 Z. W. Pan, Z. R. Dai and Z. L. Wang, *Science*, 2001, **291**, 1947.
2 M. H. Huang, S. Mao, H. Feick, H. Yan, Y. Wu, H. Kind, E. Weber, R. Russo and P. Yang, *Science*, 2001, **292**, 1897.
3 Z. L. Wang, *J. Phys.: Condens. Matter*, 2004, **16**, R829.
4 Y. W. Heo, D. P. Norton, L. C. Tien, Y. Kwon, B. S. Kang, F. Ren, S. J. Pearton and J. R. LaRoche, *Mater. Sci. Eng. R*, 2004, **47**, 1.
5 Ü. Özgür, Y. I. Alivov, C. Liu, A. Teke, M. A. Reshchikov, S. Dogan, V. Avrutin, S. J. Cho and H. Morkoc, *J. Appl. Phys.*, 2005, **98**, 041301.
6 G. C. Yi, C. Wang and W. I. Park, *Semicond. Sci. Technol.*, 2005, **20**, S22.
7 Z. Y. Fan and G. C. Lu., *J. Nanosci. Nanotech.*, 2005, **5**, 1561.
8 H. J. Fan, P. Werner and M. Zacharias, *Small*, 2006, **2**, 700.
9 A. B. Djurišić and Y. H. Leung, *Small*, 2006, **2**, 944.
10 X. D. Wang, J. H. Song and Z. L. Wang, *J. Mater. Chem.*, 2007, **17**, 711.
11 C. Klingshirn, *Phys. Stat. Sol.*, 2007, **244**, 3027.
12 L. Schmidt-Mende and J. L. MacManus-Driscoll, *Mater. Today*, 2007, **10**, 40.
13 J. Goldberger, R. He, Y. F. Zhang, S. Lee, H. Q. Yan, H. J. Choi and P. Yang, *Nature*, 2003, **422**, 599.
14 H. Shin, D. K. Jeong, J. Lee, M. M. Sung and J. Kim, *Adv. Mater.*, 2004, **16**, 1197.
15 Y. Chen, X. Xue and T. Wang, *Nanotechnology*, 2005, **16**, 1978.
16 M. Alexe, D. Hesse, V. Schmidt, S. Senz, H. J. Fan, M. Zacharias and U. Gösele, *Appl. Phys. Lett.*, 2006, **89**, 172907.

17 M. Joseph, H. Tabata and T. Kawai, *Appl. Phys. Lett.*, 1999, **74**, 2534.
18 Y. C. Yang, C. Song, X. H. Wang, F. Zeng and F. Pan, *Appl. Phys. Lett.*, 2008, **92**, 012907.
19 H. Kaga, R. Asahi and T. Tani, *Jap. J. Appl. Phys.*, 2004, **43**, 3540.
20 K. E. Sickafus, J. W. Wills and N. W. Grimes, *J. Amer. Ceram. Soc.*, 1999, **82**, 3279.
21 H. Schmalzried, *Solid State Reactions* (Weinheim, Verlag Chemie, 1974).
22 R. E. Carter, *J. Am. Ceram. Soc.*, 1961, **44**, 116.
23 E. B. Rigby and I. B. Cutler, *J. Am. Ceram. Soc.*, 1965, **48**, 95.
24 X. C. Wu, Y. Tao, Z. J. Han and B. D. Zhang, *J. Mater. Chem.*, 2003, **13**, 2649.
25 H. J. Fan, M. Knez, R. Scholz, K. Nielsch, E. Pippel, D. Hesse, U. Gösele and M. Zacharias, *Nanotechnology*, 2006, **17**, 5157.
26 B. Bengtson, R. Jagitsch and Arkiv Kemi, *Mineral. Geol.*, 1947, **24A**, 1.
27 L. Navias, *J. Am. Ceram. Soc.*, 1961, **44**, 434.
28 D. L. Branson, *J. Am. Ceram. Soc.*, 1965, **48**, 591.
29 J. T. Keller, D. K. Agrawal and A. McKinstry, *Adv. Ceram. Mater.*, 1988, **3**, 420.
30 K. C. Hui, H. C. Ong, P. F. Lee and J. Y. Dai, *Appl. Phys. Lett.*, 2005, **86**, 152116.
31 J. P. Richter, T. Voss, D. S. Kim, R. Schoz and M. Zacharias, *Nanotechnology*, 2008, **19**, 305202.
32 M. Law, L. E. Greene, A. Radenovic, T. Kuykendall, J. Liphardt and P. Yang, *J. Phys. Chem. B*, 2006, **110**, 22652.
33 Y. Wang and K. Wu, *J. Am. Chem. Soc.*, 2005, **127**, 9686.
34 Y. Wang, Q. Liao, H. Lei, X. P. Zhang, X. C. Ai, J. P. Zhang and K. Wu, *Adv. Mater.*, 2006, **18**, 943.
35 L. Zhao, M. Yosef, E. Pippel, H. Hofmeister, M. Steinhart, U. Gösele and S. Schlecht, *Angew. Chem. Int. Ed.*, 2006, **45**, 8042.
36 H. J. Fan, M. Knez, R. Scholz, K. Nielsch, E. Pippel, D. Hesse, M. Zacharias and U. Gösele, *Nature Mater.*, 2006, **5**, 627.
37 H. J. Fan, U. Gösele and M. Zacharias, *Small*, 2007, **3**, 1660.
38 F. Aldinger, *Acta Metal.*, 1974, **22**, 923.
39 Y. Yang, D. S. Kim, M. Knez, R. Scholz, A. Berger, E. Pippel, D. Hesse, U. Gösele and M. Zacharias, *J. Phys. Chem. C*, 2008, **112**, 4068.
40 Y. Yang, D. S. Kim, R. Scholz, M. Knez, S. M. Lee, U. Gösele and M. Zacharias, *Chem. Mater.*, 2008, **20**, 3487.
41 Y. Li, G. W. Meng, L. D. Zhang and F. Phillipp, *Appl. Phys. Lett.*, 2000, **76**, 2011.
42 C. H. Liu, J. A. Zapien, Y. Yao, X. M. Meng, C. S. Lee, S. S. Fan, Y. Lifshitz and S. T. Lee, *Adv. Mater.*, 2003, **15**, 838.
43 Z. Y. Fan, D. Dutta, C. J. Chien, H. Y. Chen, E. C. Brown, P. C. Chang and J. G. Lu, *Appl. Phys. Lett.*, 2006, **89**, 213110.
44 J. Grabowska et al., *Thin Solid Films*, 2008, **516**, 1725.
45 H. J. Fan, M. Knez, R. Scholz, D. Hesse, K. Nielsch, M. Zacharias and U. Gösele, *Nano Lett.*, 2007, **7**, 993.
46 S. Itoh, H. Toki, Y. Sato, K. Morimoto and T. Kishino, *J. Electrochem. Soc.*, 1991, **138**, 1509.
47 I. K. Jeong, H. L. Park and S. Mho, *Solid State Commun.*, 1998, **105**, 179.
48 Y. E. Lee, D. P. Norta, C. Park and C. M. Roulean, *J. Appl. Phys.*, 2001, **89**, 1653.
49 L. E. Shea, R. K. Datta and J. J. Brown, Jr., *J. Electrochem. Soc.*, 1994, **141**, 1950.
50 P. D. Rack, J. J. Peterson, M. D. Potter and W. Park, *J. Mater. Res.*, 2001, **16**, 1429.
51 S. Y. Bae, H. W. Seo, C. W. Na and J. H. Park, *Chem. Commun.*, 2004, **16**, 1834.
52 P. Feng, J. Y. Zhang, Q. Wan and T. H. Wang, *J. Appl. Phys.*, 2007, **102**, 074309.
53 S. Y. Bae, J. Lee, H. Jung, J. Park and J. P. Ahn, *J. Am. Chem. Soc.*, 2005, **127**, 10802.
54 K. W. Chang and J. J. Wu, *J. Phys. Chem. B*, 2005, **109**, 13572.
55 Y. J. Li, M. Y. Lu, C. W. Wang, K. M. Li and L. J. Chen, *Appl. Phys. Lett.*, 2006, **88**, 143102.
56 U. K. Gautam, Y. Bando, J. Zhan, P. M. F. J. Costa, X. S. Fang and D. Golberg, *Adv. Mater.*, 2008, **20**, 810.
57 S. K. Manik, P. Bose and S. K. Pradhan, *Mater. Chem. Phys.*, 2003, **82**, 837.
58 Y. Yang, X. W. Sun, B. K. Tay, J. X. Wang, Z. L. Dong and H. M. Fan, *Adv. Mater.*, 2007, **19**, 1839.
59 Y. Yang et al., submitted for publication.
60 B. Tan, E. Toman, Y. G. Li and Y. Y. Wu, *J. Am. Chem. Soc.*, 2007, **129**, 4162.
61 A. Rong, X. P. Gao, G. R. Li, T. Y. Yan, H. Y. Zhu, J. Q. Qu and D. Y. Song, *J. Phys. Chem. B*, 2006, **110**, 14754.
62 J. S. Jie, G. Z. Wang, X. H. Han, J. P. Fang, Q. X. Yu, Y. Liao, B. Xu, Q. T. Wang and J. G. Hou, *J. Phys. Chem. B*, 2004, **108**, 8249.
63 J. X. Wang et al., *J. Cryst. Growth*, 2004, **267**, 177.
64 H. Y. Chen, J. X. Wang, H. C. Yu, H. X. Yang, S. S. Xie and J. Q. Li, *J. Phys. Chem. B*, 2005, **109**, 2573.
65 J. X. Wang et al., *Solid State Commun*, 2004, **131**, 435.
66 J. X. Wang, X. W. Sun, S. S. Xie, W. Zhou and Y. Yang, *Crystal Growth & Design*, 2008, **8**, 707.
67 L. S. Wang, X. Z. Zhang, X. Liao and W. G. Yang, *Nanotechnology*, 2005, **16**, 2928.
68 H. S. Kim, S. O. Hwang, Y. Myung, J. Park, S. Y. Bae and J. P. Ahn, *Nano Lett.*, 2008, **8**, 551.
69 S. Jeedigunta, M. K Singh, A. Kumar and M. Shamsuzzoha, *J. Nanosci. Nanotechnol.*, 2007, **7**, 486.
70 H. L. Zhu, D. R. Yang, G. X. Yu, H. Zhang, D. L. Jin and K. H. Yao, *J. Phys. Chem. B*, 2006, **110**, 7631.
71 J. J. Urban, J. E. Spanier, L. Ouyang, W. S. Yun and H. Park, *Adv. Mater.*, 2003, **15**, 423.
72 P. M. Rørvik, A. Almli, A. T. J. van Helvoort, R. Holmestad, T. Tybell, T. Grande and M. A. Einarsrud, *Nanotechnology*, 2008, **19**, 225605.
73 Y. B. Mao, T. J. Park and S. S. Wong, *Chem. Commun.*, 2005, 5721.
74 Q. H. Xiong, J. Wang and P. C. Eklund, *Nano Lett.*, 2006, **6**, 2736.
75 M. Mattila, T. Hakkarainen, H. Jiang, E. I. Kauppinen and H. Lipsanen, *Nanotechnology*, 2007, **18**, 155301.
76 J. M. Bao, D. C. Bell, F. Capasso, J. B. Wagner, T. Mårtensson, J. Trägårdh and L. Samuelson, *Nano Lett.*, 2008, **8**, 836.
77 K. Sano, T. Akiyama, K. Nakamura and T. Ito, *J. Cryst. Growth*, 2007, **301–302**, 862.
78 F. M. Davidson, D. C. Lee, D. D. Fanfair and B. A. Korgel, *J. Phys. Chem. C*, 2007, **111**, 2929.
79 Z. H. Zhang, F. F. Wang and X. F. Duan, *J. Cryst. Growth*, 2007, **303**, 612.
80 U. Philipose, A. Saxena, H. ERuda, P. J. Simpson, Y. Q. Wang and K. L. Kavanagh, *Nanotechnology*, 2008, **19**, 215715.
81 D. H. Wang, D. Xu, Q. Wang, Y. J. Hao, G. Q. Jin, X. Y. Guo and K. N. Tu, *Nanotechnology*, 2008, **19**, 215602.
82 J. Ho, H. Hamdeh, Y. Chen, S. Lin, Y. Yao, R. Willey and S. Oliver, *Phys. Rev. B*, 1995, **52**, 10122.
83 W. Schiessl et al., *Phys. Rev. B*, 1996, **53**, 9143.
84 S. A. Oliver, V. G. Harris, H. H. Hamdeh and J. C. Ho, *Appl. Phys. Lett.*, 2000, **76**, 2761.
85 F. Grasset, N. Labhsetwar, D. Li, D. C. Park, N. Saito, H. Haneda, O. Cador, T. Roisnel, S. Mornet, E. Duguet, J. Portier and J. Etourneau, *Langmuir*, 2002, **18**, 8209.
86 M. Hofmann, S. J. Campbell, H. Ehrhardt and R. Feyerherm, *J. Mater. Sci.*, 2004, **39**, 5057.
87 C. W. Yao et al., *J. Phys. Chem. C*, 2007, **111**, 12274.
88 J. S. Jung, Y. K. Jung, E. M. Kim, S. H. Min, J. H. Jun, L. M. Malkinski, Y. Barnakov, L. Spinu and K. Stokes, *IEEE Transactions On Magnetics*, 2005, **41**, 3403.
89 S. X. Liu, B. Yue, K. Jiao, Y. Zhou and H. Y. He, *Mater. Lett.*, 2006, **60**, 154.
90 B. A. Hernandez, K. S. Chang, E. R. Fisher and P. K. Dorhout, *Chem. Mater.*, 2002, **14**, 480.
91 J. Bachmann, J. Jing, M. Knez, S. Barth, H. Shen, S. Mathur, U. Gösele and K. Nielsch, *J. Am. Chem. Soc.*, 2007, **129**, 9554.
92 S. Q. Zhou, K. Potzger, H. Reuther, G. Talut, F. Eichhorn, J. von Borany, W. Skorupa, M. Helm and J. Fassbender, *J. Phys. D: Appl. Phys.*, 2007, **40**, 964.
93 L. Tian, X. F. Yang, P. Lu, I. D. Williams, C. H. Wang, S. Y. Ou, C. L. Liang and M. M. Wu, *Inorg. Chem.*, 2008, **47**, 5522.
94 K. Raidongia and C. N. R. Rao, *J. Phys. Chem. C.*, 2008, **112**, 13366.
95 H. Martinho, N. O. Moreno and J. A. Sanjurjo et al., *Phys. Rev. B*, 2001, **64**, 024408.
96 S. Zhuiyko, T. Ono, N. Yamazoe and N. Miua, *Solid State Ionics*, 2002, **152–153**, 801.
97 F. Marumo and Y. Syono, *Acta Cryst.*, 1971, **B27**, 1868.

98 L. M. Xiong, J. L. Shi, J. L. Gu, W. H. Shen, X. P. Dong, H. R. Chen, L. X. Zhang, J. H. Guo and M. L. Ruan, *Small*, 2005, **1**, 1044.
99 X. D. Wang, C. J. Summers and Z. L. Wang, *Adv. Mater.*, 2004, **16**, 1215.
100 J. Zhou, J. Liu, X. Wang, J. Song, R. Tummala, N. S. Xu and Z. L. Wang, *Small*, 2007, **3**, 622.
101 X. L. Xu, P. Wang, Z. M. Qi, H. Ming, J. Xu, H. T. Liu, C. S. Shi, G. Lu and W. K. Ge, *J. Phys.: Condens. Matter*, 2003, **15**, L607.
102 H. J. Fan, A. Lotnyk, R. Scholz, Y. Yang, D. S. Kim, S. Senz, E. Pippel, D. Hesse and M. Zacharias, *J. Phys. Chem. C*, 2008, **112**, 6770.
103 M. Y. Tsai, C. Y. Yu, C. C. Wang and T. P. Perng, *Cryst. Growth & Design*, 2008, **8**, 2264.
104 M. Lorenz, E. M. Kaidashev, A. Rahm, T. Nobis and J. Lenzner, *Appl. Phys. Lett.*, 2005, **86**, 143113.
105 M. Zhi, L. Zhu, Z. Ye, F. Wang and B. Zhao, *J. Phys. Chem. B*, 2005, **109**, 23930.
106 H. C. Hsu, C. Y. Wu, H. M. Cheng and W. F. Hsieh, *Appl. Phys. Lett.*, 2006, **89**, 013101.
107 R. Kling, C. Kirchner, T. Gruber, F. Reuss and A. Waag, *Nanotechnology*, 2004, **15**, 1043.
108 A. Ohtomo, M. Kawasaki and T. Koida, *Appl. Phys. Lett.*, 1998, **72**, 2466.
109 A. Tsukazaki, A. Ohtomo, T. Kita, Y. Ohno, H. Ohno and M. Kawasaki, *Science*, 2007, **315**, 1388.
110 W. I. Park, G. C. Yi, M. Kim and S. J. Pennycook, *Adv. Mater.*, 2003, **15**, 526.
111 C. Kim, W. I. Park, G. C. Yi and M. Kim, *Appl. Phys. Lett.*, 2006, **89**, 113106.
112 C. Czekalla et al., *Nanotechnology*, 2008, **19**, 115202.
113 X. Y. Xue, P. Feng, Y. G. Wang and T. H. Wang, *Appl. Phys. Lett.*, 2007, **91**, 022111.
114 J. P. Liu, Y. Y. Li, X. T. Huang, G. Y. Li and Z. K. Li, *Adv. Funct. Mater.*, 2008, **18**, 1448.
115 Y. Sharma, N. Sharma, G. V. Subba Rao and B. V. R. Chowdari, *Adv. Funct. Mater.*, 2007, **17**, 2855.
116 M. A. Cameron, I. P. Gartland, J. A. Smith, S. F. Diaz and S. M. George, *Langmuir*, 2000, **16**, 7435.
117 M. Knez, K. Nielsch and L. Niinistö, *Adv. Mater.*, 2007, **19**, 3425.
118 D. W. Zeng, C. S. Xie, M. Dong, R. Jiang, X. Chen, A. H. Wang, J. B. Wang and J. Shi, *Appl. Phys. A*, 2004, **79**, 1865.

